Anatomy of the Akhmediev breather: cascading instability, first formation time and Fermi-Pasta-Ulam recurrence

Siu A. Chin[†], Omar A. Ashour[‡], Milivoj R. Belić[‡]

[†]*Department of Physics and Astronomy,*

Texas A&M University, College Station, TX 77843, USA and

[‡]*Science Program, Texas A&M University at Qatar, P.O. Box 23874 Doha, Qatar*

Abstract

By invoking Bogoliubov's spectrum, we show that for the nonlinear Schrödinger equation, the modulation instability of its $n = 1$ Fourier mode on a finite background automatically triggers a further cascading instability, forcing all the higher modes to grow exponentially in locked-step with the $n = 1$ mode. This fundamental insight, the enslavement of all higher modes to the $n = 1$ mode, explains the formation of a triangular-shaped spectrum which generates the Akhmediev breather, predicts its formation time analytically from the initial modulation amplitude, and shows that the Fermi-Pasta-Ulam (FPU) recurrence is just a matter of energy conservation with a period twice the breather's formation time. For higher order MI with more than one initial unstable modes, while most evolutions are expected to be chaotic, we show that it is possible to have isolated cases of "super-recurrence", where the FPU period is much longer than that of a single unstable mode.

I. INTRODUCTION

The study of modulation instability (MI) in solutions of the nonlinear Schrödinger equation on a constant background has became a cornerstone of modern nonlinear physics, underlying many of the advances in understanding deep water wave propagation [1–3], plasma physics [4], light transmission in optical fibers [5], and the formation of optical rogue waves [6, 7]. While directly solving the nonlinear Schrödinger numerically is a relatively simple matter [3], exact solutions to the nonlinear Schrödinger equation on a finite background, known as the Akhmediev [8, 9] and Kuznetsov-Ma [10, 11] breathers (ABs, KMBs), have provided much insight into the subsequent evolution of MI in these solutions. In this work, we seek to provide a more detailed understanding of the Akhmediev breather's formation, its fundamental structure and its remarkable mode of evolution.

Akhmediev breathers [8, 9] are exact solutions to the cubic nonlinear Schrödinger

$$i\frac{\partial\psi}{\partial t}+\frac{1}{2}\frac{\partial^2\psi}{\partial x^2}+|\psi|^2\psi=0 \tag{1}$$

on a finite background, $|\psi(t\to\pm\infty)|\to 1$. In this work, we show that: 1) The modulation instability of the $n=1$ Fourier mode, automatically triggers a further *cascading instability*, forcing all the higher modes to grow exponentially in locked-step with the $n=1$ mode. This results in a *triangular spectrum* [14], which is *the* signature of the Akhmediev breather. The remarkable simplicity of the Akhmediev breather is that, once formed, this triangular spectrum basically evolves intact, throughout its subsequent evolution, oblivious to any nonlinear interactions. 2) By knowing the analytical form of the Fourier amplitudes from AB, one can predict the time of the breather's first formation. This formation time corresponds to the maximum compression distance [15] in an optical fibre, and is an important design parameter for breather productions. Our formation time is an improvement over that derived in Ref.[15]; it is accurate even for purely real modulation amplitudes. 3) Since all higher Fourier modes are "enslaved" [16] to the $n=1$ mode, there is no freedom for the equal partition of energy and no Fermi-Pasta-Ulam [17, 18] (FPU) paradox. The FPU recurrence is then just a consequence of bound state energy conservation with a period twice the breather's formation time. 4) In cases of higher-order modulated instabilities, where there are multiple initial unstable modes, super FPU recurrences are possible, but Fourier amplitudes beyond the first AB-like peak are no longer predicted by the Akhmediev breather.

II. ANATOMY OF THE AKHMEDIEV BREATHER

The Akhmediev breather [8, 9]

$$\psi(t,x) = \frac{(1-4a)\cosh(\lambda t) + \sqrt{2a}\cos(\Omega x) + i\lambda\sinh(\lambda t)}{\sqrt{2a}\cos(\Omega x) - \cosh(\lambda t)}, \tag{2}$$

is an exact solution to (1) parametrized by a single real positive parameter a, which fixes the wave number Ω and the growth factor λ. In order to make clear the most fundamental aspect of the solution, it is best to regard a as parametrizing the solution's periodic length L:

$$L = \frac{\pi}{\sqrt{1-2a}}. \tag{3}$$

For an AB, a ranges between 0 and 1/2; at $a = 1/2$ the Peregrine soliton [19] forms, with an infinite periodic length. Given L, the spacing in k-space is $\Delta k = 2\pi/L$, so that the allowed k vectors are just

$$k_n = n\Delta k \qquad \text{for} \quad n = 0, \pm 1, \pm 2, \cdots. \tag{4}$$

The wave number Ω of the Akhmediev breather (2) then corresponds to the fundamental, $n = 1$ mode

$$\Omega = \Delta k = 2\pi/L = 2\sqrt{1-2a}, \tag{5}$$

and the growth factor

$$\lambda = \sqrt{8a(1-2a)}, \tag{6}$$

is due to the instability of this mode, as determined by the Bogoliubov spectrum [12].

While the general Benjamin-Feir [1] instability is known since 1967, the modulation instability of the cubic nonlinear Schrödigner equation is known from Bogoliubov's work on the uniform Bose gas [12, 13] since 1947. This is because a uniform Bose gas can be described by the Gross-Pitaevskii equation [13, 20], which is just the cubic nonlinear Schrödinger equation with a uniform background.

Bogoliubov's spectrum [12, 13] for the elementary excitations of a uniform Bose gas is given by

$$\varepsilon_k = \sqrt{E_k(E_k + 2U)} \tag{7}$$

where $E_k = k^2/2$ is the free-particle energy and $U = g|\psi|^2$. In the repulsive (defocusing) case of $g = +1$, all elementary excitations are stable. In the attractive (focusing) case of

$g = -1$, all k-modes with plane-wave e^{ikx} are unstable if $E_k + 2U < 0$. In the latter case, for a constant background $|\psi|^2 = 1$, the $n = \pm 1$ modes are unstable with imaginary frequencies

$$\varepsilon_{\pm 1} = \pm i\sqrt{\frac{\Delta k^2}{2}(2 - \frac{\Delta k^2}{2})} = \pm i\sqrt{8a(1-2a)} = \pm i\lambda, \tag{8}$$

and the modulus of the amplitudes $A_{\pm 1}$ grows in time as

$$|A_{\pm 1}| \propto \mathrm{e}^{\mp i\varepsilon_{\pm 1} t} = \mathrm{e}^{\lambda t}. \tag{9}$$

Thus, the instability of the $n = \pm 1$ modes determines the growth factor λ. More generally, since a k-mode is unstable for $E_k - 2 < 0$, this means that all modes with $k_n < 2$, or $n\Omega < 2$, are unstable. For $1 < \Omega < 2$ only one mode is unstable. If $\Omega < 1$, then there will be more than one unstable mode with more than one growth factor. The case of $\Omega = 1$ corresponds to $a = 3/8 = 0.375$, hence there will be multiple unstable modes initially if $a > 0.375$.

When starting with a constant background of $\psi = 1$, with $A_0 = 1$ and $A_{n\neq 0} = 0$, any minute perturbation which triggers the instability of the $n = 1$ mode will cause it to grow exponentially, according to (9). This is the standard Benjamin-Feir [1] scenario. What has not been explicitly stated prior to this work is that, for the nonlinear Schrödinger equation, this growth of the $n = 1$ mode will *automatically* trigger a *cascading instability* of all the higher modes, causing all to grow exponentially, locked to the fundamental mode. This is because the Bogoliubov spectrum is obtained by linearizing

$$|\psi|^2 = |A_0 + A_1 \mathrm{e}^{i\Delta kx} + A_{-1}\mathrm{e}^{-i\Delta kx}|^2 \tag{10}$$

to leading orders in $A_{\pm 1}$. The final equation is of the form

$$i\partial_t A_{\pm 1} \propto A_{\pm 1}, \tag{11}$$

which results in an exponential growth factor. Doing the same expansion for $A_{\pm 2}$ in

$$|\psi|^2 = |A_0 + A_1 \mathrm{e}^{i\Delta kx} + A_{-1}\mathrm{e}^{-i\Delta kx} + A_2\mathrm{e}^{i2\Delta kx} + A_{-2}\mathrm{e}^{-i2\Delta kx}|^2 \tag{12}$$

now yields leading order contributions of the form

$$i\partial_t A_{\pm 2} \propto A_{\pm 1}^2 A_0^* + 2A_0 A_{\pm 1} A_{\mp 1}^*, \tag{13}$$

which are simply proportional to a product of two $A_{\pm 1}$. This is because the amplitudes $A_{\pm 2}$ are just starting to grow from zero, and are much smaller than the constant $A_0 \approx 1$ and the

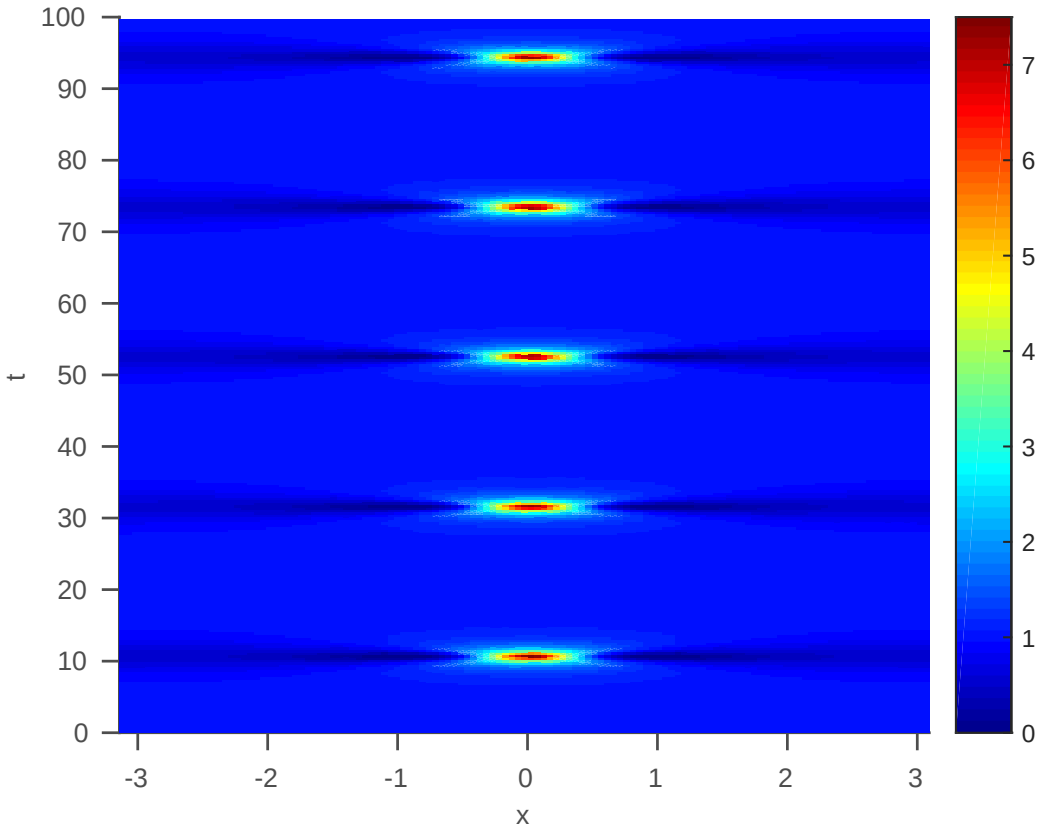

FIG. 1. (color online) Density $|\psi(t,x)|^2$ plot of the numerical solution of the cubic nonlinear Schrödinger equation (1) using a second-order splitting method with $\Delta t = 0.0001$ for $a = 3/8$ and initial profile (17).

already growing $A_{\pm 1}$. Thus $A_{\pm 2}$ are given by a simple *time integration*,

$$A_{\pm 2} \propto \int (A_{\pm 1}^2 A_0^* + 2A_0 A_{\pm 1} A_{\mp 1}^*) dt \tag{14}$$

resulting in

$$|A_{\pm 2}| \propto |A_1|^2 \propto \mathrm{e}^{2\lambda t}. \tag{15}$$

Repeating similar argument for $A_{\pm n}$ $(n \neq 0)$ then yields

$$|A_{\pm n}| = C_n \mathrm{e}^{|n|\lambda t} = C_n |A_1|^{|n|}. \tag{16}$$

Therefore the growth of the entire spectrum is dictated by the growth of $|A_1|$. If C_n does not grow exponentially faster than n, then at $t < 0$, $\ln(|A_{\pm n}|) \propto -|n|$, which is triangular-shaped spectrum [14] in n.

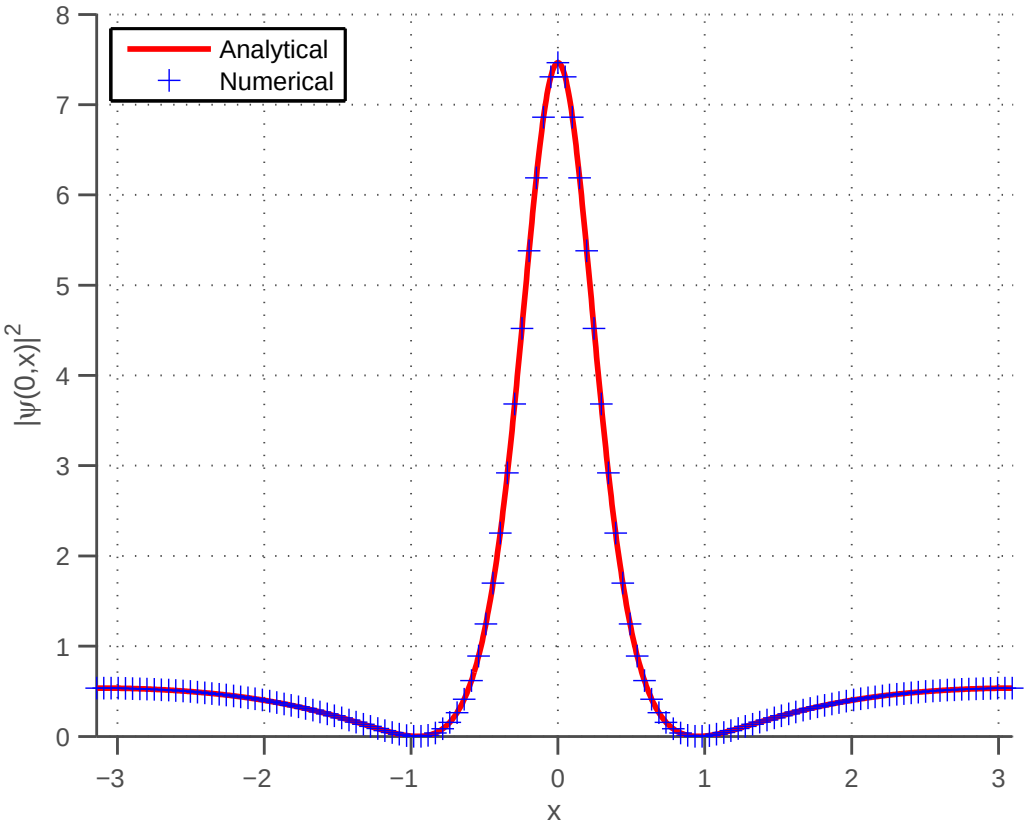

FIG. 2. (color online) The first breather's numerical spatial profile from the calculation of Fig. 1 as compared to the analytical form of $|\psi(0,x)|^2$ from Eq. (2).

To check the validity of this cascading scenario, we solve the nonlinear Schrödinger equation numerically using a second-order splitting method for the case of $a = 3/8$, $L = 2\pi$, $\Delta k = 1$, $\Omega = 1$, $\lambda = \sqrt{3}/2$, with an initial profile

$$\psi(0,x) = A_0 + A_1 e^{i\Omega x} + A_1 e^{-i\Omega x} = A_0 + 2A_1 \cos(\Omega x), \tag{17}$$

where $A_0 = \sqrt{1-2A_1^2}$ and $A_1 = 10^{-4}$, so that wave function is normalized as in Ref. [8]:

$$\frac{1}{L}\int_0^L |\psi(0,x)|^2 dx = A_0^2 + 2A_1^2 = 1. \tag{18}$$

The allowed k-modes are just integers $k = n = 0, \pm 1, \pm 2$, *etc.*. In Fig. 1, the resulting density profile plot shows that the breather is first formed at $t \sim 10$ and then recurs later at intervals of $t \sim 20$. To verify that the structure formed is precisely the breather of (2) with $a = 3/8$, we compare in Fig. 2, the structure's spatial profile at the formation time with $|\psi(0,x)|^2$ of Eq.(2). The agreement is exact.

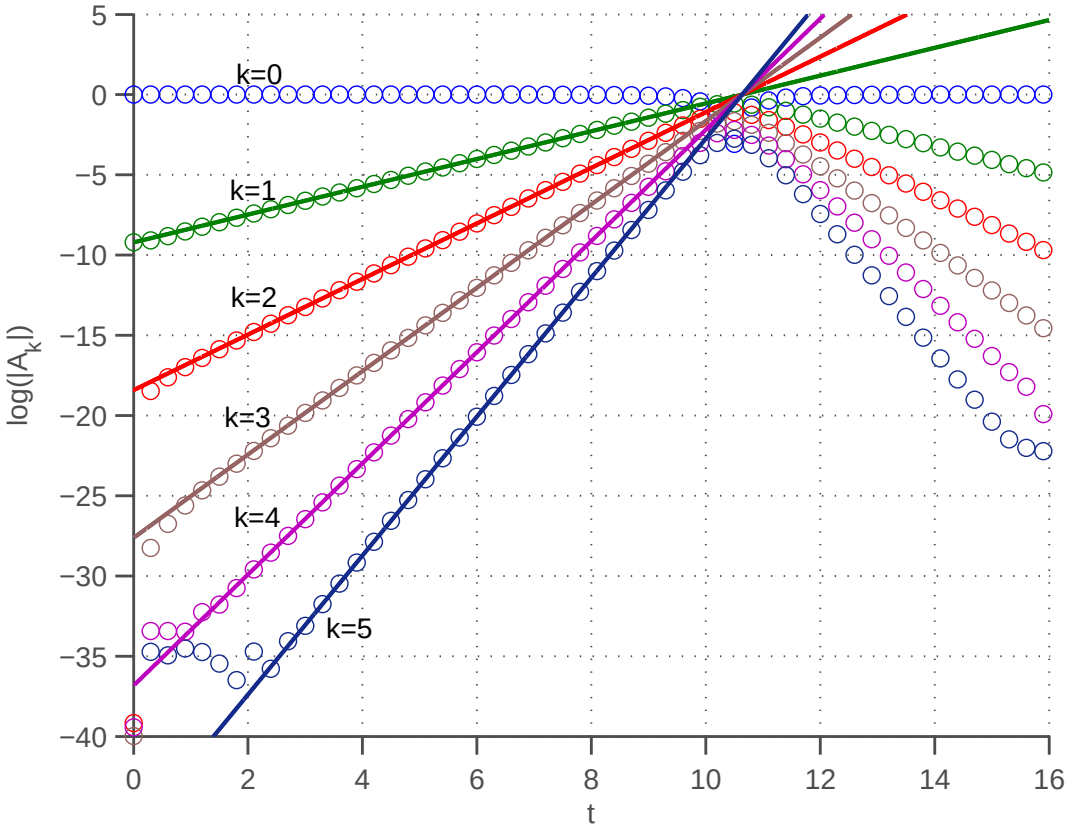

FIG. 3. The growth of the $k = 1 - 5$ Fourier amplitudes in time. Symbols are numerical results from the calculation of Fig. 1. Solid lines are $k\lambda(t - t_c)$ with $\lambda = \sqrt{3}/2$ and $t_c = 10.6352$.

In Fig. 3, the growth of $|A_k|$ for $k = 1 - 5$ is compared to the cascading prediction (16) that $|A_k| = \mathrm{e}^{k\lambda(t-t_c)}$, with the prefactor C_n absorbed into the shift of the time origin t_c. All $k = 1 - 5$ amplitudes can be well-fitted with a single cascading time of $t_c = 10.6352$,

$$\ln(|A_k|) = |k|\lambda(t - t_c), \tag{19}$$

where t_c is the time needed for A_1 to grow from an initial value of 10^{-4} to unity at the rate of $\lambda = \sqrt{3}/2$,

$$t_c = -\frac{\ln(A_1)}{\lambda} = 10.6352. \tag{20}$$

The excellent linear fits to the amplitudes in Fig. 3 are therefore parameter-free predictions of the cascading instability. It only fails to describe the growth of the amplitudes near and after the amplitudes' peak, at which time the exact dynamics takes over. The breather's

actual formation time of

$$t_0 = 10.4691 \tag{21}$$

will be derived in a later section; the cascading time t_c is just a first estimate of t_0. Because of the cascading instability, the growth of the amplitudes is best understood and plotted in terms of $\ln(|A_k|)$ rather than $|A_k|$ or $|A_k|^2$.

Of course, this exponential growth in the amplitudes cannot continue indefinitely, since it must be constrained by the unitary condition on the wave function:

$$|A_0|^2 + 2\sum_{n>1} |A_n|^2 = 1. \tag{22}$$

If one assumes that the cascading spectrum (16) persists (setting $C_n = 1$) even when $|A_1|$ can no longer be considered as "small", then since $|A_0|$ can only be depleted to zero, the maximum that $|A_1|$ can grow to is given by

$$\sum_{n>1} (|A_1|^2)^n = \frac{1}{2} \quad \Rightarrow \quad max(|A_1|) = \frac{1}{\sqrt{3}} \tag{23}$$

and $max(|A_n|) = (1\sqrt{3})^n$. As we will see in the later sections, after the amplitudes have reached their maxima, by energy conservation, they must decline back to their starting values, in a time-symmetric image of their rise.

To see how exactly the Akhmediev breather forms from this cascading scenario, we now compute the exact amplitudes $A_n(t)$ from the solution (2). From Eq. (2), we have

$$\begin{aligned} A_n(t) &= \frac{1}{L}\int_0^L \psi(t,x)\cos(n\Omega x)dx, \\ &= \frac{1}{2\pi}\int_0^{2\pi}\Big(1 + \frac{2(1-2a)\cosh(\lambda t) + i\lambda\sinh(\lambda t)}{\sqrt{2a}\cos(y) - \cosh(\lambda t)}\Big)\cos(ny)dy, \\ &= \frac{1}{2\pi}\int_0^{2\pi}\Big(1 + \frac{2(1-2a) + i\lambda\tanh(\lambda t)}{\alpha\cos(y) - 1}\Big)\cos(ny)dy, \end{aligned} \tag{24}$$

where we have defined

$$\alpha = \sqrt{2a}/\cosh(\lambda t) < 1,$$

and where

$$\frac{1}{2\pi}\int_0^{2\pi}\frac{\cos(ny)}{\alpha\cos(y) - 1}dy = -\frac{1}{\sqrt{1-\alpha^2}}\Big(\frac{1-\sqrt{1-\alpha^2}}{\alpha}\Big)^n. \tag{25}$$

Therefore, one has

$$A_0(t) = 1 - \frac{2(1-2a) + i\lambda\tanh(\lambda t)}{\sqrt{1-\alpha^2}}, \tag{26}$$

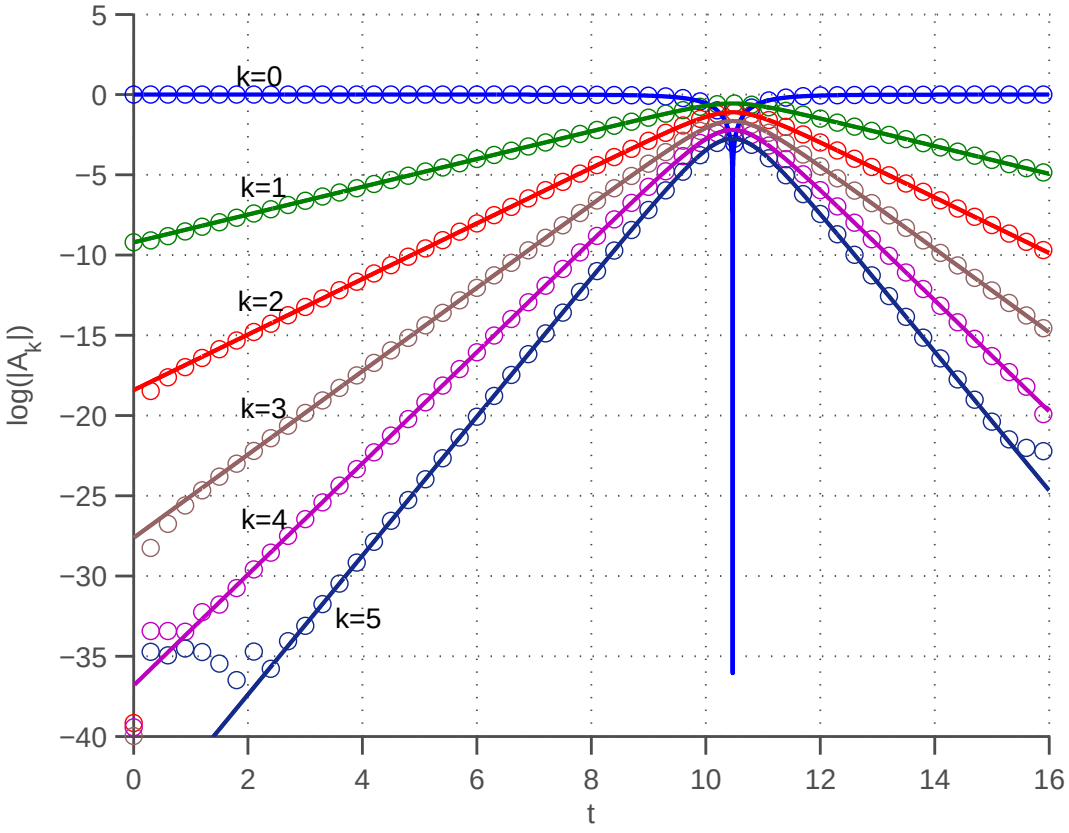

FIG. 4. The growth of the $k = 0-5$ Fourier amplitudes as compared to the exact amplitudes (26) and (27). The numerical data are the same as those in Fig. 3. The plunging vertical line depicts the total depletion of A_0 (=0) at $t = t_0$.

and for $n \neq 0$,

$$A_n(t) = -\frac{2(1-2a) + i\lambda \tanh(\lambda t)}{\sqrt{1-\alpha^2}} \left(\frac{1-\sqrt{1-\alpha^2}}{\alpha} \right)^{|n|}. \tag{27}$$

This derivation agrees with the original results of Akhmediev and Korneev [8] (up to an overall sign) for $a = 1/4$, and with others [21], but not with the amplitudes given in Ref. [14].

Equation (27) means that all amplitudes are phase-locked to that of $A_1(t)$ and their magnitudes simply decrease geometrically with increasing n:

$$A_n(t) = \left(\frac{1-\sqrt{1-\alpha^2}}{\alpha} \right)^{|n|-1} A_1(t). \tag{28}$$

This affirms the cascading scenario, but the Akhmediev breather goes further in asserting that all $|n| > 1$ amplitudes evolve in locked-step with $A_1(t)$ at *all times*. In 1981, Infeld

[16] explained the success of his truncated three-wave model as due to the "enslavement" of higher modes to the $n = 1$ modes. This conjecture is precisely confirmed by the Akhmediev breather and is the basis for the qualitative success of all three-wave models [16, 22]. This "enslavement" is a remarkably simple mechanism of nonlinear evolution.

Note that

$$A_0(0) = 1 - 2\sqrt{1-2a} = 1 - \Omega \tag{29}$$

and for $n \neq 0$,

$$A_n(0) = -2\sqrt{1-2a}\Big(\frac{1-\sqrt{1-2a}}{\sqrt{2a}}\Big)^{|n|}. \tag{30}$$

Therefore, the depletion of the background is maximal, $A_0(0) = 0$, only for $a = 3/8$, $\Omega = 1$. We now plot $\ln(|A_k(t-t_0)|)$ in Fig. 4, using the exact AB amplitudes of (26) and (27). The exact amplitudes match the numerical data perfectly.

When the time origin is shifted by $t \to t - t_0$, then for $t << t_0$

$$\alpha \to 2\sqrt{2a}\mathrm{e}^{\lambda(t-t_0)} \to 0$$

and

$$|A_n(t-t_0)| \to 2\sqrt{1-2a}\Big(\sqrt{2a}\mathrm{e}^{\lambda(t-t_0)}\Big)^{|n|}. \tag{31}$$

Therefore, at any a the Akhmediev breather will yield a growing triangular spectrum, as predicted by the cascading instability, but with a known prefactor C_n.

III. THE FORMATION TIME

The excellent match in Fig. 4 between numerical data and theoretical results means that one can track $\ln(|A_1(t-t_0)|)$ back to $t = 0$, and set it equal to the initial amplitude,

$$\ln A_1 = \ln(|A_1(-t_0)|), \tag{32}$$

and directly determine t_0 from the initial amplitude! From Fig. 4, for A_1 small it is clear that $\ln(|A_1(t-t_0)|)$ is in the linearly growing region. There is no need to use the full expression (27); the approximation (31)

$$|A_1(-t_0)| = \lambda \mathrm{e}^{-\lambda t_0} \tag{33}$$

is sufficient. One then has an analytical form for the formation time:

$$t_0 = -\frac{\ln(A_1/\lambda)}{\lambda} = -\frac{\ln(A_1)}{\lambda} + \frac{\ln\lambda}{\lambda}. \tag{34}$$

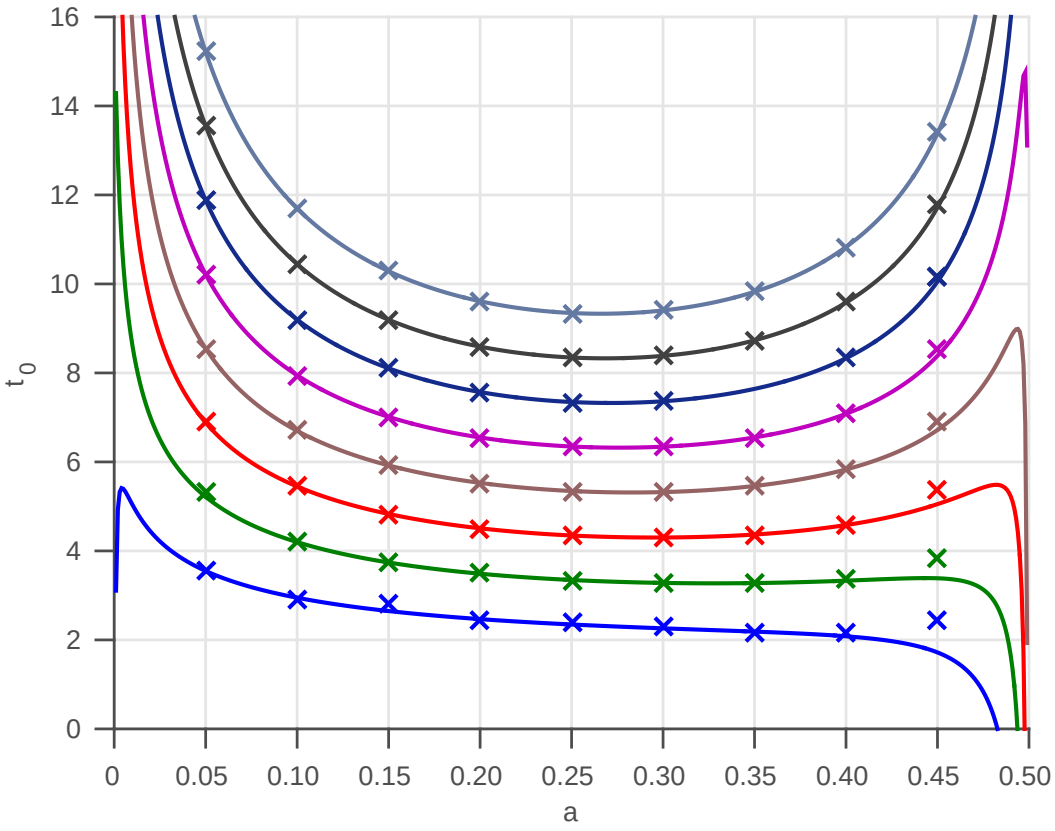

FIG. 5. The corrected Akhmediev breather's first formation times as functions of a for various initial amplitudes parametrized as $A_1 = \mathrm{e}^{-w}$. Crosses are numerical values; lines are analytical estimates of (35). From the top to the bottom are results corresponding to $w = 9 - 2$.

Setting $A_1 = 10^{-4}$ gives $t_0 = 10.6352 - 0.1661 = 10.4691$, in exact agreement with the observed formation time of (21).

The analytical formation time (34) is exact for $A_1 \to 0$. It is surprising to find that (34) remains a good approximation at $a = 3/8$ even for A_1 as large as ≈ 0.1. However, at larger values of A_1, there is not enough time for the cascading process to build up to the triangular spectrum, and the resulting evolution is no longer described by the Akhmediev breather. Thus, in order for the Akhmediev breather and (34) to be applicable, the smaller the initial modulating amplitude, the better.

The above discussion for t_0 is only for the case of $a = 3/8$, $\Omega = 1$. It turns out that for $\Omega \neq 1$, another correction is necessary. This is due to the fact that for $\Omega \neq 1$, the numerical $\ln(|A_1(t)|)$ will start out either steeper or flatter than the slope λ. In general, starting

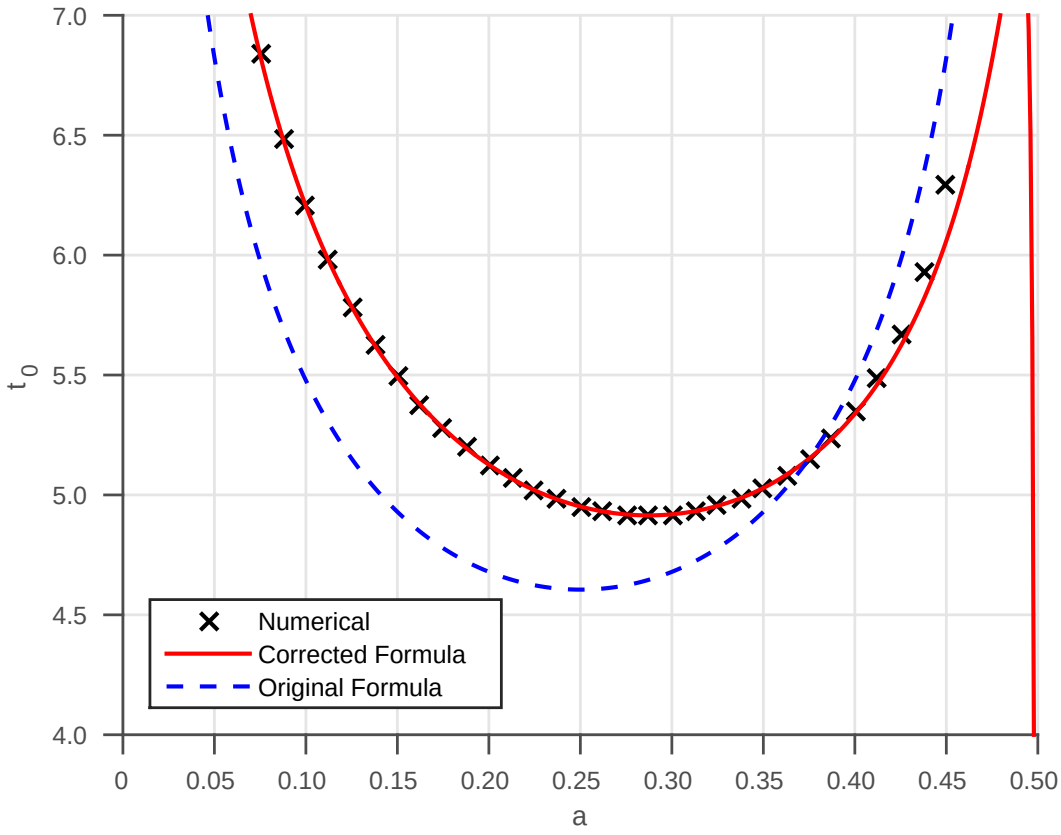

FIG. 6. Comparing the original formula (34) and the corrected formula (35) for the formation time t_0 at A_1=0.01.

with a finite $A_1 \neq 0$, unless the initial A_1 is very small, $\ln(|A_1(t)|)$ is not described by the Akhmediev breather. But if we are using the straightline portion (33) of the Akhmediev breather to determine t_0 approximately, then we must use a value of $|A_1|$ logarithmically higher or lower, to match the slope. The correction, found empirically, takes a very simple form:

$$t_0 = -\frac{\ln[A_1/(\lambda\Omega)]}{\lambda} = -\frac{\ln(A_1)}{\lambda} + \frac{\ln\lambda}{\lambda} + \frac{\ln\Omega}{\lambda}. \tag{35}$$

In Fig. 5, we compare the numerical formation time for various values of the modulating amplitude A_1 and a. At smaller values of A_1, $w = 7, 8, 9$, the agreement is excellent even at $a > 0.375$, where there are more than one initial unstable modes. Naturally, the analytical estimates fail as one approaches $a = 1/2$, where the AB scenario is not applicable anymore and the Peregrine soliton scenario takes over.

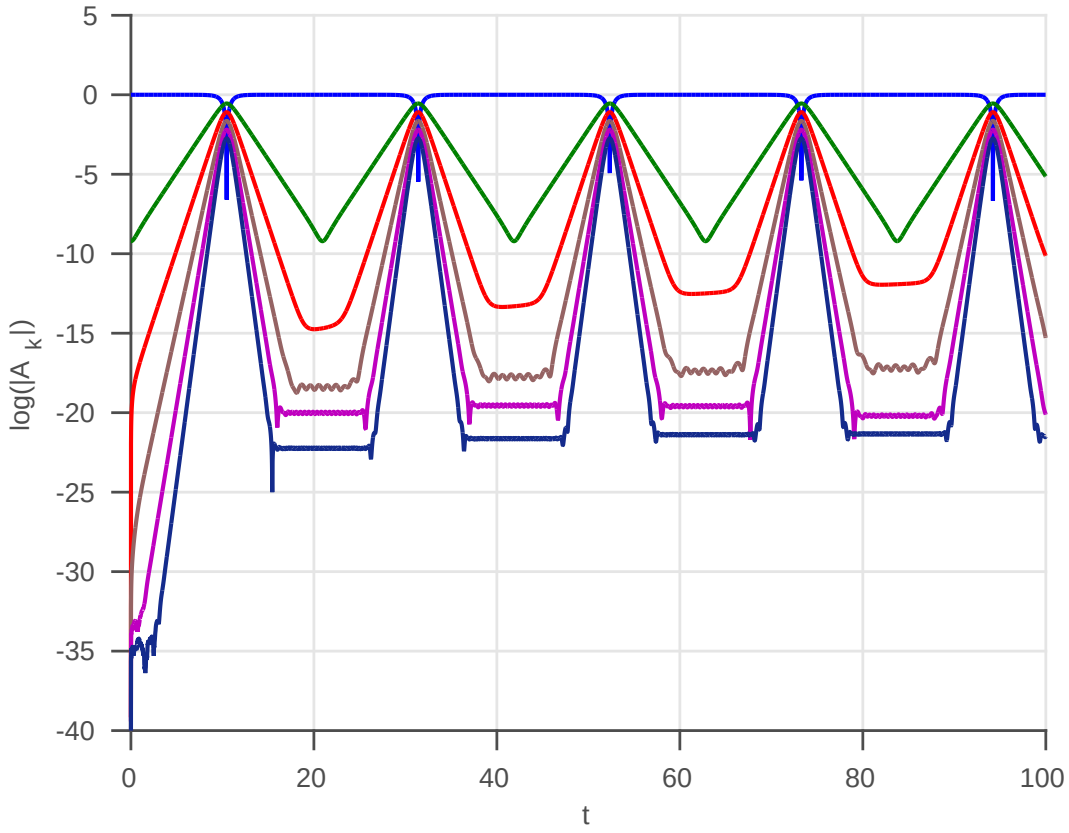

FIG. 7. The evolution of the $k = 0 - 5$ Fourier amplitudes (top to bottom) beyond the first peak.

At $A_1 = 0.01$, we compare both (34) and (35) in Fig. 6 for all values of a. The old formula (34) is only correct at one point, $a = 3/8 = 0.375$ or $\Omega = 1$. The corrected formula (35) is in excellent agreement with numerical results, even at this relatively large value of A_1. If one interprets t as z, the distance along the optical length, then t_0 corresponds to the distance at which A_0 is maximally depleted. This is called the maximum compression distance by Erkintalo *et al.* in Ref. [15]. They have also derived the formation time (34) by an entirely different expansion method. Our use of the amplitude $|A_1(t)|$ from (31) seemed more direct. Figure 6 is to be compared with Fig. 3 in Ref. [15].

IV. FERMI-PASTA-ULAM RECURRENCE

In Fig. 7, we show the continued evolution of the amplitudes for the case of $a = 3/8$ after the first peak. One sees that A_1 decreases back to its initial value and repeats its

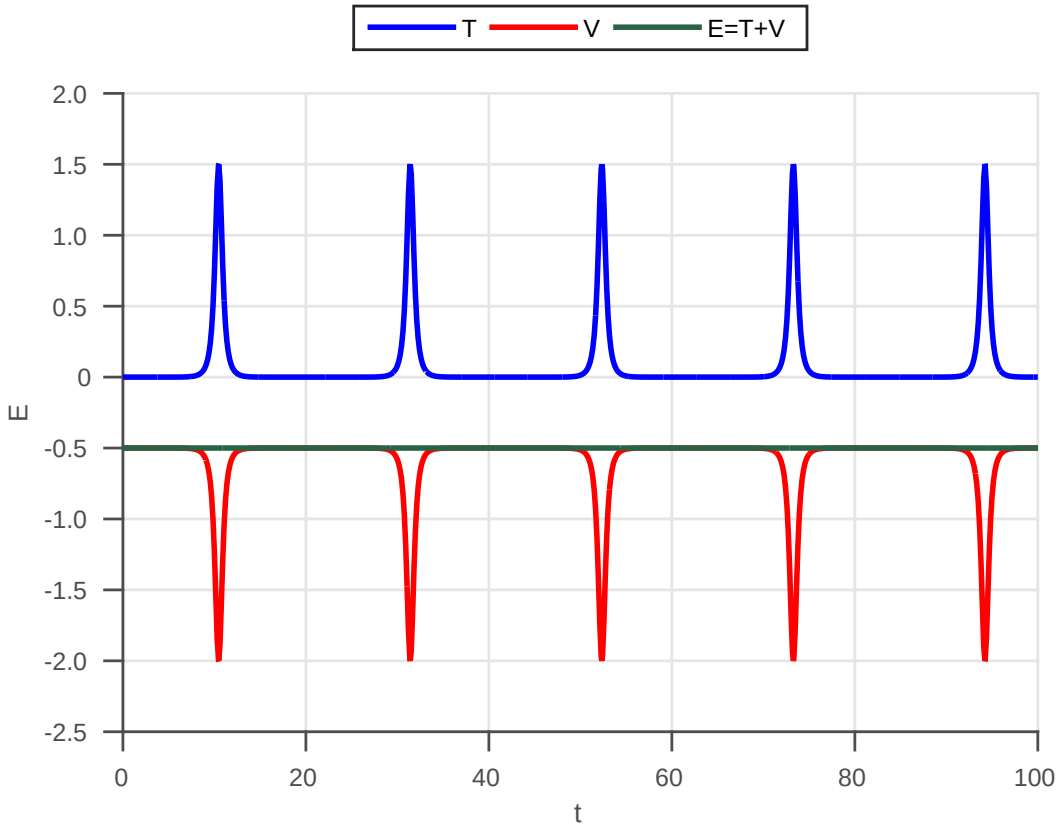

FIG. 8. The kinetic energy (top) and the potential energy (bottom) of the nonlinear Schrödinger equation with initial wave function (17). The line nearly identitical to -1/2 is the total energy.

initial growing pattern. This is the celebrated Fermi-Pasta-Ulam [17, 18] recurrence of the nonlinear Schrödinger equation, known from the early experimental work of Lake *et al.* [2] and the numerical calculations of Yuen and Ferguson [3]. As discussed earlier, in AB, all higher amplitudes should rise and fall in locked-step with A_1. However, due to the algorithm's error and limited numerical precision, this locked-step is difficult to maintain when the amplitudes are near zero. (A_2 is specially difficult here because it is neutrally stable with a zero growth rate. It tends to drift more than other modes.) The exact AB is of no help in explaining this recurrence, since the exact wave function (2) only describes a single rise and fall of the breather. The key to understanding this recurrence is energy conservation.

In Fig. 8 we, plot the kinetic energy T, the potential energy V, and the total energy $E = T + V$ of the nonlinear Schrödinger equation (1) as a function of t, where T and V are

defined by

$$T = \frac{1}{L}\int_0^L dx\, \psi^*(t,x)(-\frac{1}{2}\partial_x^2)\psi(t,x) = \sum_k \frac{1}{2}k^2|A_k(t)|^2,$$
$$V = -\frac{1}{2}\frac{1}{L}\int_0^L dx\, |\psi(t,x)|^4.$$

At the peak of the AB, (29) and (30) give $A_0 = 0$ and

$$|A_k|^2 = \frac{1}{3^k}, \tag{36}$$

and hence

$$T = 2\sum_{k=1}^{\infty}|A_k|^2\frac{1}{2}k^2 = \sum_{k=1}^{\infty}\frac{k^2}{3^k} = \frac{3}{2}. \tag{37}$$

This exlains why the kinetic energy peaks at 1.5.

One immediately recognizes that energy patterns in Fig. 8 are typical of a bound state collision with a hard-wall potential, like that of a bouncing ball released from rest at a given height, then falling to the ground. When the ball hits the ground, its velocity and kinetic energy are at their respective maxima. When the ball begins to bounce back elastically, its velocity reverses direction and both its magnitude and the kinetic energy decrease back to zero. When the ball reaches back its original height with zero kinetic energy, it begins to fall again. Thus every kinetic energy peak is a moment of impact. The FPU period is therefore just the period of the bouncing ball, which is twice the time for it to fall to the ground. Hence,

$$t_{\rm FPU} = 2t_0 = 2\Big(-\frac{\ln[A_1/(\lambda\Omega)]}{\lambda}\Big). \tag{38}$$

This is clearly seen in the first optical observation of the FPU recurrence [23].

In the original observation of Yuen and Ferguson [3], recurrence in the nonlinear Schrödinger is liken to the work of Fermi-Pasta-Ulam [17], because it was thought that energy is being distributed from A_0 to infinite-many higher Fourier modes. If all these higher modes interact *independently*, then the energy will thermalize and impossible to reassemble back to A_0. From AB, we now have a simple explanation of this recurrence: *All* higher modes are locked-in, to rise and fall with $A_{\pm1}(t)$ at all times. There are therefore no infinite number of degrees of freedom to distribute energy, no entropy to destroy time-reversal symmetry. Recurrence is just a matter of simple energy conservation for basically two degrees of freedom, $A_0(t)$ and $A_1(t)$, similar to that of a two-body collision problem.

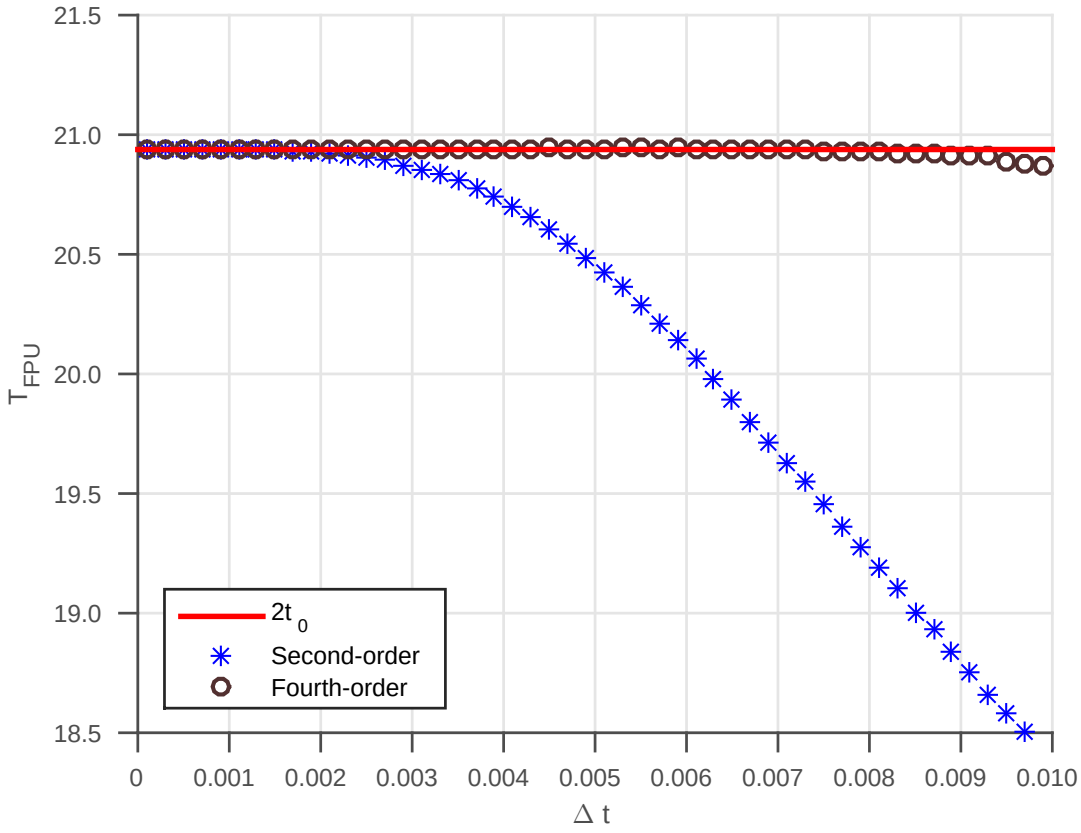

FIG. 9. The Fermi-Pasta-Ulam recurrence period $t_{\rm FPU}$ as determined by a second (stars) and a fourth-order (circles) splitting scheme with $\Delta t = 0.01$ to 0.0001 at $a = 3/8$ for an initial amplitude of $A_1 = 10^{-4}$. The horizontal red line is the predicted FPU period of $2t_0$.

If one were to numerically determine the period of the bouncing ball accurately, then the ball must be able to return to its original height accurately. In other words, energy conservation is paramount. For the wave function (17), the sum of kinetic and potential energy initially is

$$E_0 = A_1^2 - \frac{1}{2} - 4A_1^2 + 7A_1^4. \tag{39}$$

Since $A_1^4 = 10^{-16}$, the total energy is near the limit of double-precision. For $A_1 < 10^{-4}$, the total energy would be beyond the limit of double-precision and cannot be accurately conserved numerically (unless higher precision software is used).

To demonstrate the importance of energy conservation, we plot in Fig. 9, the FPU recurrence period using a second and a fourth-order splitting algorithm with $\Delta t = 0.01$ to 0.0001. With decreasing Δt, as the second algorithm is increasingly more accurate,

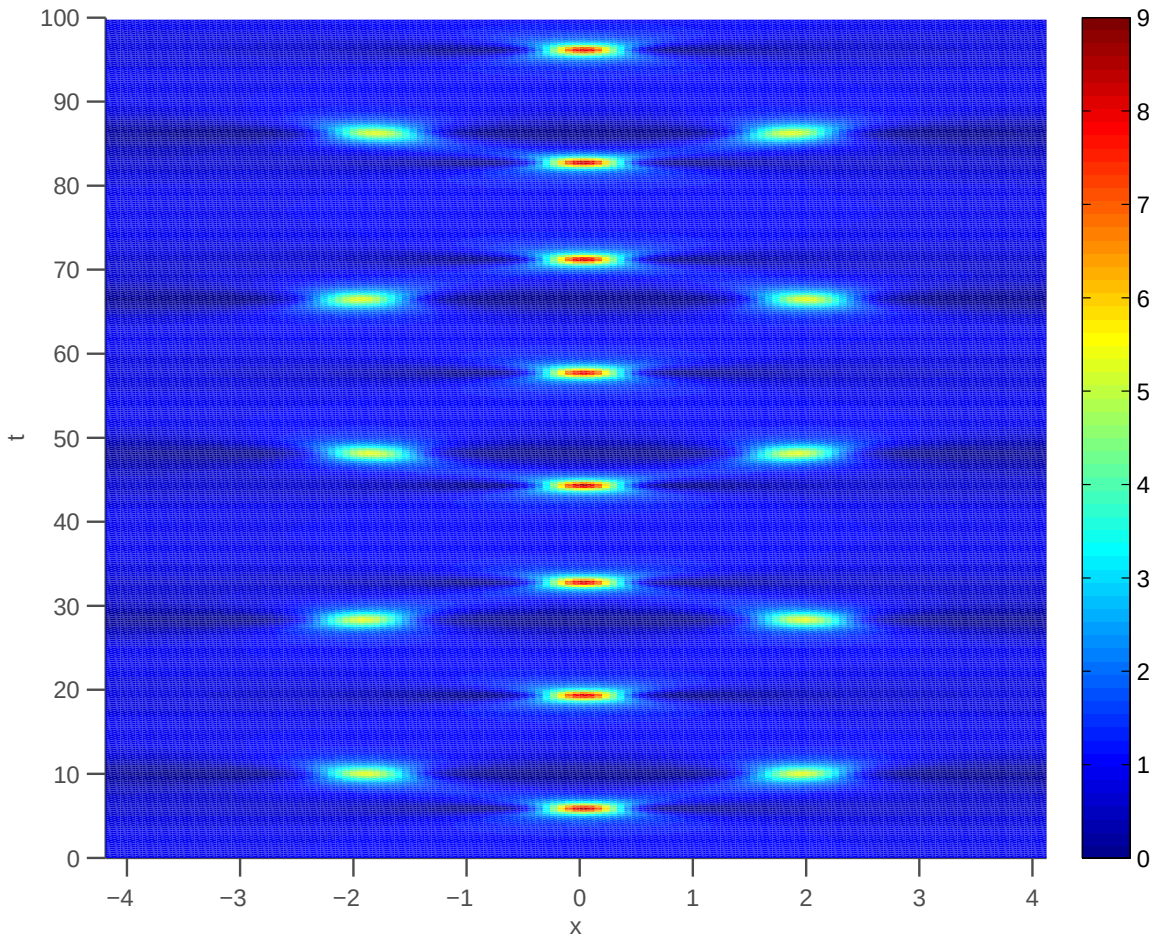

FIG. 10. Density $|\psi(t,x)|^2$ plot for $a = 55/128$.

its numerical FPU period approaches the expected value of $2t_0$ from below, and does not converge until $\Delta t < 0.002$. However, the same converged value can be obtained by using a fourth-order algorithm at step size as large as $\Delta t = 0.008$. Also, as shown by the second order algorithm, when energy conservation is less accurate, the FPU period tends to shorten.

V. HIGHER-ORDER MODULATION INSTABILITY

After understanding simple FPU recurrences in the last section, we can now tackle the more complicated case of higher-order modulated instablility, with multiple initial unstable modes.

Consider the case of $a = 55/128 = 0.4296875$, where the fundamental wave number

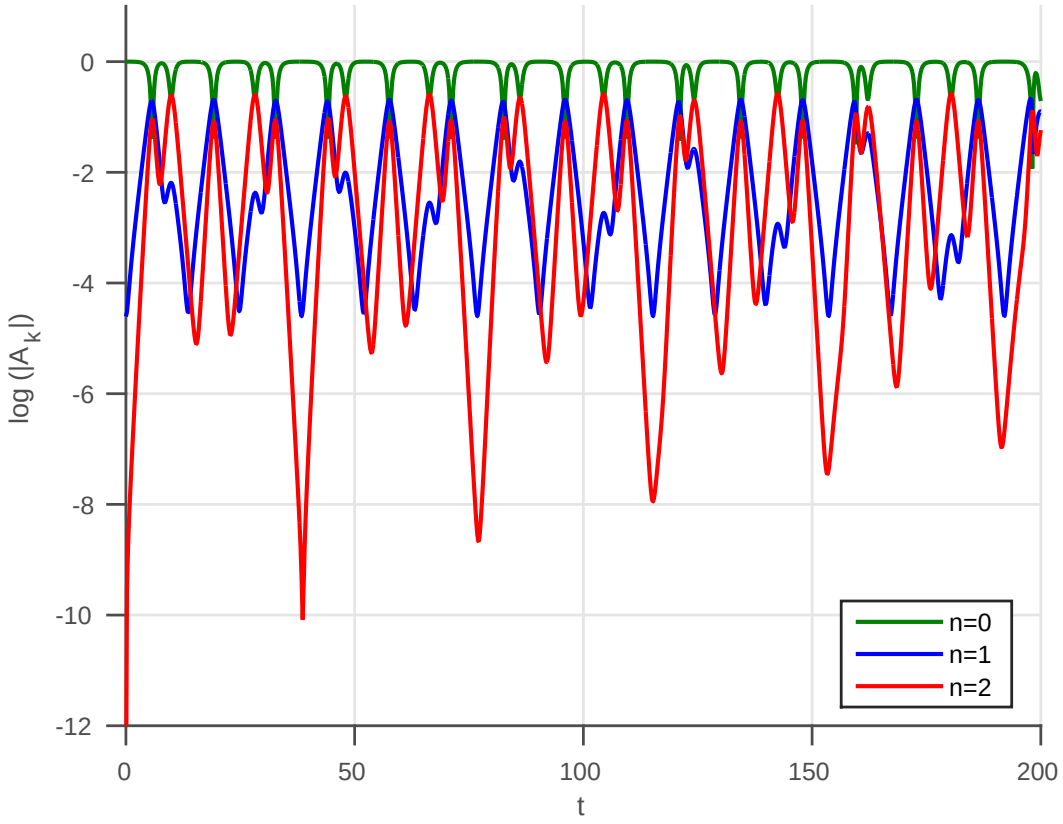

FIG. 11. Evolving amplitude plot for $a = 55/128$ with the super-recurrence period most clearly seen in the oscillation of the $n = 2$ amplitude.

$\Omega_1 = 3/4$ and its first harmonic $\Omega_2 = 3/2$ are both unstable, according to the Bogoliubov spectrum, with respective growth factors $\lambda_1 = 0.6953$ and $\lambda_2 = 0.9922$. This is the case studied in Ref. [24]. In Fig.10, we show the resulting density plot when the initial modulating amplitude A_1 is 0.01. A short simulation with $t < 15$ would only show one breather near $t \sim 5$ and two breathers near $t \sim 10$. However, the long time simulation of Fig. 10 reveals that there is "super-recurrence" with the period $t_{FPU} \sim 40$! This is more clearly shown in Fig. 11, where for clarity, we only plotted the amplitudes of the first three modes. The longer period of $t_{FPU} \approx 38.4$ is clearly visible in the oscillation of the $n = 2$ amplitude.

Even for $A_1 = 0.01$, the cascading instability still enslaves all the higher modes, including the unstable $n = 2$ mode. This is because under the cascading instability, the $n = 2$ mode will grow at a rate of $2(0.6953) = 1.3906$, which is faster than its own rate of 0.9922. As a

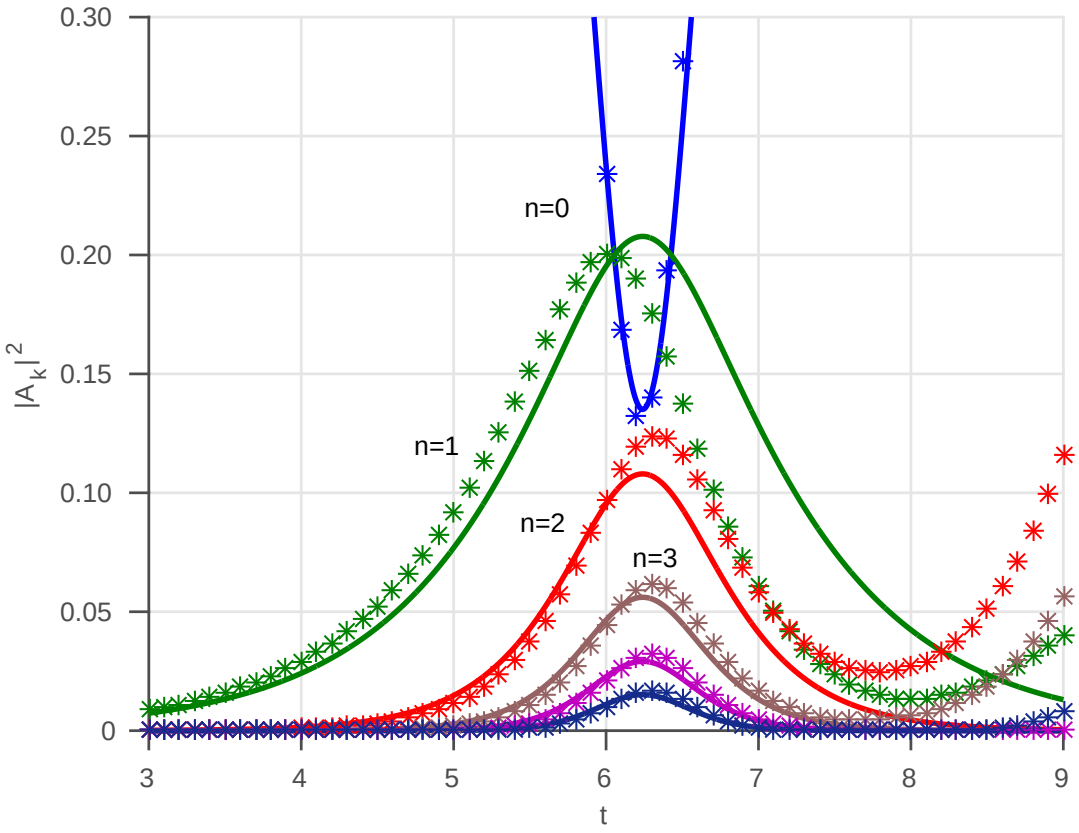

FIG. 12. Comparing amplitude intensity of the Akhmediev breather (lines) with numerical results (stars) for $a = 0.45$.

consequence, an Akhemdiev breather will form at

$$t_0 = -\frac{\ln(A_1)}{\lambda} + \frac{\ln\lambda}{\lambda} + \frac{\ln\Omega}{\lambda}$$
$$= 6.6233 - 0.5227 - 0.4138 = 5.6868. \tag{40}$$

This is in reasonable agreement with the observed value of $t_0 = 5.759$, given the fact that $A_1 = 0.01$ is not small enough for the analytical formula to hold. This time difference at $a \approx 0.43$ is already noticeable in Fig. 6.

After the first peak, all amplitudes decline, as in an Akhemdiev breather, but since the $n = 2$ mode is intrinsically unstable, it starts to grow at its own rate while A_1 is still declining. The result is the formation of a twin-peak breather near $t \approx 9.9$, where $n = 2$ has the largest amplitude. Wabnitz and Akhmediev [25] have noted that this can be an efficient way of transferring power from the pump or the background to the $n = 2$ mode. After this peak, the amplitdues decline and rise again, to form another Akhemdiev breather

near $t \approx 19.2$. This peak is at mid-period, and the A_1 amplitude retrace its step back to its starting value at the "super-recurrence" period of $t_{FPU} \approx 38.4$. This period is even more clearly seen in the $n = 2$ amplitude, where it is the time at which A_2 declines back to zero. It would be of interest to see whether this super-recurrence period can be seen analytically in the solutions obtained by Darboux transformation in Ref. [24].

Because of its instability, the amplitude of the $n = 2$ mode after the first peak is markedly different from that of an Akhmediev breather. In Fig. 12, we compare AB at $a = 0.45$ with numerical results for $A_1 = 0.01$. This case has *three* unstable initial modes. The evolution before the first peak, because of the cascading instability, remain AB-like, however, after the peak, numerical results for the intensity of the $n = 1$ and $n = 2$ mode are below and above that of AB's profile respectively. This is to be compared with Fig. 3 of Ref. [21]. Hammani *et al.* [21] are correct in asserting that AB dynamics remained qualitatively useful in describing various mode intensities in approaching the first peak. However, their Fig. 3 also clearly shows that their data after the intensity peak, while still in agreement with numerical solutions of the nonlinear Schrödinger equation similar to our Fig. 12, are no longer quantitatively described by the Akhmediev breather. Thus, while there are many areas where AB can give an excellent account of light propagation and generation [26], AB dynamics is insufficient to describe higher-order modulation instabilities *beyond* the first peak. With more than two unstable modes, that dynamics fast becomes chaotic.

VI. CONCLUSIONS

In this work, we have exposed in detail the anatomy of producing the Akhmediev breather, that it is basically the result of a cascading instability, which enslaved all higher modes to evolve in locked-step with the $n = 1$ mode. This at once makes plain that FPU recurrence is just a necessary consquence of energy conservation. By giving an analytical formula for the breather's first formation time beyond that of AB, we have also derived an accurate analytical estimate of the FPU period. In cases of higher-order modulation instability, where there are multiple unstable initial modes, we showed that due to the interplay between and among various unstable modes, super-recurrences are possible. However, such recurrences are beyond the simple description of AB (2) and may require the use of Darboux transformations [24] to give an analytical account of such periodicities.

Because of the cascading instability, we were led to plot *not* the mode intensities $|A_n|^2$ themselves, but $\ln(|A_n|)$. As evident from Figs. 3, 4, 7 and 11, these log-plots of amplitudes give the clearest description of the nonlinear evolution of ABs of the Schrödinger equation. This will be equally useful for understanding other modulation-instability related nonlinear evolutions. Further work is necessary to understand the higher-order MI of ABs, as well as the emerging complex dynamics associated with MI of Peregrine and of KMBs.

ACKNOWLEDGMENTS

This publication was made possible by NPRP GRANT #5-674-1-114 from the Qatar National Research Fund (a member of Qatar Foundation). MRB acknowledges support by the Al-Sraiya Holding Group.

---

[1] T. B. Benjamin, J. Feir, "The disintegration of wave trains on deep water, part 1 Theory", J. Fluid Mech. 27 (1967) 417-430

[2] B. M. Lake, H. C. Yuen, H. Rungaldier and W. E. Ferguson, "Nonlinear deep-water waves: theory and experiment. Part 2. Evolution of a continuous wave train", J. Fluid Mech. (1977) 49-74.

[3] H. C. Yuen and W. E. Ferguson, Jr., "Relationship between Benjamin-Feir instability and recurrence in the nonlinear Schrödinger equation", Phys. Fluids, **21**, 1275-1278 (1978).

[4] T. Taniuti and H. Washimi, "Self-Trapping and Instability of Hydromagnetic Waves Along the Magnetic Field in a Cold Plasma", Phys. Rev. Lett. 21 (1968) 209.

[5] K. Tai, A. Hasegawa, and A. Tomita, "Observation of modulational instability in optical fibers", Phys. Rev. Lett. 56(2), 135-138 (1986).

[6] D. R. Solli, C. Ropers, P. Koonath, and B. Jalali, "Optical rogue waves", Nature 450, 1054 (2007).

[7] J. M. Dudley, F. Dias, M. Erkintalo, and G. Genty, "Instabilities, breathers and rogue waves in optics", Nature Phot. 8, 755 (2014).

[8] N. Akhmediev and V. Korneev, "Modulation instability and periodic solutions of the nonlinear Schrödinger equation", Theor. Math. Phys. 69 (1986) 1089-1093.

[9] N. Akhmediev, V. Eleonskii, and N. Kulagin, "Exact first-order solutions of the non- linear Schrödinger equation", Theor. Math. Phys. 72 (1987) 809-818.

[10] E. A. Kuznetsov, "Solitons in a parametrically unstable plasma", Sov. Phys. Dokl. 22, 507 (1977).

[11] Y.C. Ma, "The perturbed plane-wave solution of the cubic Schrdinger equation", Stud. Appl. Math. 60, 43 (1979).

[12] N. N. Bogoliubov, "On the theory of superuidity", J. Phys. (USSR) 11, 23 (1947), reprinted in D. Pine, *The Many-Body Problem* (Benjamin, New York, 1961), p. 292.

[13] A. L. Fetter and J. D. Walecka, *Quantum Theory of Many-Particle Systems*, McGraw-Hill, New York, 1971, pp. 317, 493-496.

[14] N. Akhmediev, A. Ankiewicz, J. M. Soto-Crepo, and J. M. Dudley, "Universal triangular spectra in parametrically-driven systems" Phys. Lett. A **375**, 775-779 (2011).

[15] M. Erkintalo, G. Genty, B. Wetzel and J. M. Dudley, "Akhmediev breather evolution in optical fiber for realistic initial conditions" Phys. Lett. 375 (2011) 2029-2034.

[16] E. Infeld, "Quantitive theory of the Fermi-Pasta-Ulam recurrence in the nonlinear Schrödinger equation", Phys. Rev. Lett. 47 (1981) 717718

[17] E. Fermi, J. Pasta, and S. Ulam, in *Collected Papers of Enrico Fermi*, edited by E. Segre (Univ. of Chicago Press, Chicago, 1965) Vol. 2, p. 978.

[18] J. Ford, "The Fermi-Pasta-Ulam problem: Paradox turns discovery", Phys. Rep. 213, 271 (1992).

[19] D. H. Peregrine, "Water waves, nonlinear Schrdinger equations and their solutions", J. Aust. Math. Soc. B25, 16 (1983).

[20] C. J. Pethick and H. Smith, *Bose-Einstein Condensation in Dilute Gases*, (Cambridge University Press, Cambridge, 2002), p.172.

[21] K. Hammani, B. Wetzel, B. Kibler, J. Fatome, C. Finot, G. Millot, N. Akhmediev, and J. M. Dudley, "Spectral dynamics of modulation instability described using Akhmediev breather theory", Opt. Lett. 36 (2011) 2140-2142.

[22] S. Trillo and S. Wabnitz, "Dynamics of the nonlinear modulational instability in optical fibers", Opt. Lett. 16 (1991) 986-988.

[23] G. Van Simaeys, P. Emplit, and M. Haelterman, "Experimental demonstration of the Fermi-Pasta-Ulam recurrence in a modulationally unstable optical wave", Phys. Rev. Lett. 87 (2001)

033902.

[24] M. Erkintalo, K. Hammani, B. Kibler, C. Finot, N. Akhmediev, and J.M. Dudley, G. Genty, "Higher-order modulation instability in nonlinear fiber optics", Phys. Rev. Lett. 107 (2011) 253901

[25] S. Wabnitz and N. Akhmediev, "Efficient modulation frequency doubling by induced modulation instability" Optics Comm. 283 (2010) 1152-1154.

[26] J. M. Dudley, G. Genty, F. Dias, B. Kibler, and N. Akhmediev, "Modulation instability, Akhmediev breathers and continuous wave supercontinuum generation", Opt. Express 17 (2009) 21497-21508.